

November 21 2017

Arsenate co-precipitation with Fe(II) oxidation products and retention or release during precipitate aging

*Anna-Caterina Senn^{a,b}, Stephan J. Hug^a, Ralf Kaegi^a, Janet G. Hering^{a,b,c}, Andreas
Voegelin^{a,*}*

^a Eawag, Swiss Federal Institute of Aquatic Science and Technology, Ueberlandstrasse 133,
CH-8600 Duebendorf, Switzerland

^b Department of Environmental Sciences, Institute of Biogeochemistry and Pollutant
Dynamics, ETH, Swiss Federal Institute of Technology, Zurich, Switzerland

^c School of Architecture Civil and Environmental Engineering, EPFL, École Polytechnique
Fédérale de Lausanne, Switzerland

* Corresponding author. E-mail address: andreas.voegelin@eawag.ch, phone +41 58 765 54
70, fax +41 58765 52 10

This document is the accepted manuscript version of the following article:
Senn, A. -C., Hug, S. J., Kaegi, R., Hering, J. G., & Voegelin, A. (2018). Arsenate co-
precipitation with Fe(II) oxidation products and retention or release during precipitate
aging. *Water Research*, 131, 334-345. <http://doi.org/10.1016/j.watres.2017.12.038>

This manuscript version is made available under the CC-BY-NC-ND 4.0
license <http://creativecommons.org/licenses/by-nc-nd/4.0/>

ABSTRACT

The co-precipitation of arsenate (As(V)) with Fe(III)-precipitates is of great importance in water treatment and critically affects the fate of As in environmental systems. We studied the effects of dissolved phosphate (P; 0-1 mM), silicate (Si; 0 or 0.5 mM) and Ca (0, 0.5 and 4 mM) on the sequestration of 7 μ M As(V) by Fe(III)-precipitates formed by the oxidation of 0.5 mM Fe(II) in aerated bicarbonate-buffered solutions with an initial pH of 7.0 as well as the retention or release of As(V) after precipitate aging for 30 d at 40 °C. Dissolved As(V) concentrations in fresh precipitate suspensions greatly varied as a function of the initial dissolved P/Fe ratio ($(P/Fe)_{init}$) and the concentrations of Ca and Si. Limited As(V) removal was observed at $(P/Fe)_{init}$ that exceeded the critical ratio $(P/Fe)_{crit}$ above which exclusively (Ca-)Fe(III)-phosphate forms. Effective As(V) removal was observed at $(P/Fe)_{init} < (P/Fe)_{crit}$, where initial formation of (Ca-)Fe(III)-phosphate is followed by the formation of Si-ferrihydrite in Si-containing electrolytes and of poorly-crystalline lepidocrocite and hydrous ferric oxide in the Si-free electrolytes. The retention of As(V) and P by fresh Fe(III)-precipitates was most effective in systems containing both Ca and Si. In the Si- and Ca-free electrolytes at $(P/Fe)_{init}$ of ~0.2-0.6, the rapid onset of precipitate aging with conversion of Fe(III)-phosphate to ferrihydrite resulted in a substantial remobilization of As(V) (up to 55% of initially precipitated As(V)). Ca reduced As remobilization during aging by stabilizing Ca-Fe(III)-phosphate and Si by stabilizing Si-ferrihydrite against transformation. Consequently, also after aging, the lowest dissolved As(V) and P fractions were observed in precipitate suspensions containing both Ca and Si.

Keywords: arsenic removal; phosphate removal; iron precipitates; precipitate aging; water treatment

1. INTRODUCTION

Arsenic (As) occurs ubiquitously in soils, sediments and natural water. Owing to the high chronic toxicity of As, elevated As concentrations of geogenic or anthropogenic origin pose a serious threat to human health, especially via the consumption of As-containing drinking water and food. More than 100 million people worldwide rely on groundwater with toxic levels of geogenic As as drinking water resource (Smedley and Kinniburgh 2002), most of them in West Bengal (India), Bangladesh and Vietnam (Murcott 2012). In these regions, As-contaminated groundwater is also widely used for the irrigation of paddy rice and other crops, which leads to the accumulation of As in soils, As transfer into the food chain, and potentially also reduced crop yields (Dittmar et al. 2010a, Dittmar et al. 2010b, Melkonian et al. 2013, Panaullah et al. 2008).

The environmental fate and impact of As is tightly coupled to the cycling of Fe. Under anoxic conditions in soils and aquifers, the reductive dissolution of Fe(III)-(hydr)oxides with adsorbed As and phosphate (P) and the reduction of strongly sorbing arsenate (As(V)) to less strongly sorbing arsenite (As(III)) result in elevated concentrations of dissolved As(III) and Fe(II) in soil porewater or groundwater (Roberts et al. 2010, Weber et al. 2010). When such waters are aerated, dissolved Fe(II) is oxidized to Fe(III) which forms poorly soluble Fe(III)-precipitates. The As(III) is (partly) co-oxidized to more strongly sorbing As(V) and (partly) removed from solution together with P, silicate (Si), Ca and other solutes by co-precipitation with Fe(III) (Hug and Leupin 2003, Roberts et al. 2004). Various Fe-based techniques for As removal from drinking water have been investigated, including co-oxidation and co-precipitation of As with naturally present or added Fe(II) (Hug et al. 2008, Meng et al. 2001, Roberts et al. 2004) or with Fe(II) produced via zerovalent Fe corrosion (Bang et al. 2005, Katsoyiannis et al. 2008, Leupin and Hug 2005, Nikolaidis et al. 2003, Su and Puls 2001b) or via electrocoagulation (Lakshmanan et al. 2009, Li et al. 2012, Ratna Kumar et al. 2004).

The uptake of As by freshly formed Fe(III)-precipitates depends on the presence or absence of the co-precipitating solutes phosphate (P) and silicate (Si) and of the major cation Ca (Delaire et al. 2017, Meng et al. 2000, Meng et al. 2002, Roberts et al. 2004, Wilkie and Hering 1996) and their interdependent effects on precipitate structure and composition (Senn et al. 2015, Voegelin et al. 2010). Whereas phosphate strongly competes with As for uptake by Fe(III)-precipitates, Ca promotes As removal via electrostatic interactions and by attenuating P competition through direct Ca-P interactions. The co-precipitation of As with Fe(III)-precipitates has been examined in a large number of studies to date. However, much of this work has been performed in the context of the treatment of mineral processing wastes and addressed As uptake and retention by Fe(III)-precipitates obtained from the forced hydrolysis of concentrated Fe(III) solutions (e.g., (Chen et al. 2009, Paktunc et al. 2008, Paktunc et al. 2015, Violante et al. 2007)). Studies concerned with As removal by Fe(III)-precipitates formed by Fe(II) oxidation under conditions relevant for natural ground and surface waters or water treatment, on the other hand, either did not consider variations in Fe(III)-precipitate structure (Roberts et al. 2004) or examined only a limited set of conditions (van Genuchten et al. 2012, van Genuchten et al. 2014b, Voegelin et al. 2010). To date, studies that systematically link the extent of As co-precipitation with Fe oxidation products to variations in precipitate structure and chemical conditions are lacking.

The aging of fresh Fe(III)-precipitates may result in structural transformations such as increasing polymerization and crystallization that can be associated with a loss of sorption capacity and consequently oxyanion release (Ford 2002, Fuller et al. 1993, Majzlan et al. 2007, Mayer and Jarrell 2000, Paktunc et al. 2008, Senn et al. 2017, Violante et al. 2007, Waychunas et al. 1993). This process is highly relevant with respect to the handling of residues from drinking water As removal and the fate of As associated with Fe(III)-precipitates in natural systems. However, the individual and combined effects of P, Si and Ca

on the transformation of Fe(II)-derived Fe(III)-precipitates and on As(V) retention during aging under conditions relevant for near-neutral ground- and surface waters have not been examined so far.

In an extensive experiment on the formation of Fe(III)-precipitates via Fe(II) oxidation at near-neutral pH and the transformation of the fresh precipitates during aging, we characterized fresh and aged Fe(III)-precipitates and identified the effects of P, Si and Ca on precipitate structure, composition and aging (Senn et al. 2015, Senn et al. 2017), as summarized in Table 1: Marked changes in precipitate formation occur at initial dissolved P/Fe ratios $(P/Fe)_{init}$ around a critical ratio $(P/Fe)_{crit}$ that depends on the background electrolyte. At $(P/Fe)_{init} > (P/Fe)_{crit}$, amorphous Fe(III)-phosphate or Ca-Fe(III)-phosphate forms, the latter exhibiting a higher maximum precipitate P/Fe ratio due to Ca-P interactions. At $(P/Fe)_{init} < (P/Fe)_{crit}$, the initial formation of (Ca-)Fe(III)-phosphate leads to the depletion of dissolved P. Subsequently, poorly-crystalline lepidocrocite and a ferrihydrite-type precipitate form in the Si-free electrolytes, and Si-rich ferrihydrite in the Si-containing electrolytes with $(Si/Fe)_{init}$ of 1. Variations in precipitate structure are reflected in variations in dissolved P. Starting from very low concentrations at $(P/Fe)_{init}$ around $(P/Fe)_{crit}$, dissolved P markedly increases with increasing $(P/Fe)_{init}$ as the uptake capacity of the (Ca-)Fe(III)-phosphate is increasingly exceeded. Below $(P/Fe)_{crit}$ in the absence of Si, immediate onset of (Ca-)Fe(III)-phosphate polymerization after dissolved P depletion leads to an increase in dissolved P fractions with decreasing $(P/Fe)_{init}$. In the presence of Si, the high sorption capacity of Si-ferrihydrite inhibits the release of P within 4 hours after the onset of Fe(II) oxidation (Senn et al. 2015). Aging of the fresh precipitates for 30 d at 40 °C in their synthesis solutions induces marked structural changes (Senn et al. 2017). Most importantly, the continuing polymerization of Fe(III) in (Ca-)Fe(III)-phosphate and ferrihydrite-type precipitates leads to a decrease of the oxyanion sorption capacity of the precipitates and thus

the remobilization of co-precipitated P (Senn et al. 2017). The extent of P remobilization however is strongly dependent on the structure of the fresh precipitate and is lowest for precipitates formed in the presence of Ca and Si, due to the stabilizing effect of Ca on Ca-Fe(III)-phosphate and of Si on Si-ferrihydrite as well as due to Ca-phosphate formation.

The present study is based on our previous work on the effects of P, Si and Ca on the structure of fresh Fe(III)-precipitates, their transformation after 30 days of aging, and consequences for P retention (Senn et al. 2015, Senn et al. 2017). Here we report on the sequestration of a trace concentration of As(V) by the fresh and aged precipitates in the same multifactorial experiment and on how As(V) sorption affects residual dissolved As(V). Furthermore, we show results from a time-resolved 35-days Fe(III)-precipitate aging experiment that provides insight into the time-dependence of As(V) and P release.

2. MATERIALS AND METHODS

2.1. Synthesis of fresh and aged precipitates with co-precipitated As(V)

Fresh and aged Fe(III)-precipitate suspensions were prepared from six background electrolytes (Na, Ca, low Ca, Mg, Na+Si and Ca+Si) at twelve P concentrations as described previously (Senn et al. 2015, Senn et al. 2017). The precipitates were synthesized at an initial pH of 7.0 by the oxidation of 0.5 mM Fe(II) in the presence of 0 to 1 mM P, corresponding to $(P/Fe)_{init}$ from 0-2. The starting solutions contained 7 μ M As(V), corresponding to an initial molar As(V)/Fe(II) ratio $((As/Fe)_{init})$ of 0.014. To focus on the effects of Fe(III)-precipitate formation and transformation on As(V) uptake and retention and to avoid the confounding effects of concomitant As(III) oxidation, all experiments reported here were conducted with As(V). Treatment labels indicate the background electrolyte and $(P/Fe)_{init}$ (e.g., Na 0.05 for experiment in Na electrolyte at $(P/Fe)_{init}$ of 0.05).

The background electrolytes were prepared by dissolving 8 mM NaHCO₃ (Na), 4 mM CaCO₃ (Ca), 0.5 mM CaCO₃ and 7 mM NaHCO₃ (low Ca), or 4 mM MgO (Mg) in high-purity doubly deionized (DDI) water (18.2 M Ωcm, Milli-Q[®] Element, Millipore) purged with CO₂ gas. To prepare the Si-containing electrolytes (Na+Si, Ca+Si), 0.5 mM Si was added from an alkaline stock solution (100 mM Si from Na₂SiO₃·9H₂O, prepared daily) to the slightly acidic Na and Ca electrolytes. The pH was then adjusted to 7.0 (±0.1) by purging with pressurized air. After pH adjustment, 7 μM (525 μg/L) As(V) and 0-1 mM P (12 concentrations) were spiked using pH-neutral stock solutions (13.35 mM Na₂HAsO₄·7H₂O and 50 mM NaH₂PO₄·H₂O; respectively). Fe oxidation and precipitation was initiated by adding 0.5 mM Fe(II) using a daily prepared acidic stock solution (50 mM FeSO₄·7H₂O, 1 mM HCl). After thorough mixing, an unfiltered aliquot was collected to determine total initial element concentrations. Subsequently, the suspensions were left for 4 h, with half-hourly remixing by turning the bottles upside down several times. After 4 h reaction time, the fresh suspensions were sampled by collecting unfiltered and filtered (0.1 μm cellulose nitrate filter membranes) aliquots for the determination of total and dissolved element concentrations, respectively (and the solids for solid phase characterization). A duplicate set of fresh suspensions (after 4 h reaction time) was transferred into an oven and aged for 30 days at 40 °C before collection of unfiltered and filtered aliquots. During aging, the pH of the suspensions increased to pH 7.9±0.3 due to CO₂ outgassing (Senn et al. 2017), as it would also occur in natural waters.

At (P/Fe)_{init} of 0.25 (0.56 mM Fe), a time-resolved aging experiment was conducted in the Na, Na+Si, Ca and Ca+Si electrolytes. Initial sample preparation and Fe(II) oxidation was performed as described above, with 200 mL of solution in 300 mL polypropylene bottles. The initial solutions were sampled unfiltered and filtered. After 4 h, filtered samples were collected again and the bottles were transferred to an oven set to 40°C to age the suspensions

for 35 days. Filtered samples were collected up to 35 days aging time (0.3, 1, 2, 3, 6, 10, 14, 21, 28, 35 d) for analysis of dissolved element concentrations and pH.

2.2. Determination of total and dissolved element concentrations

For the determination of the concentrations of Fe, P, As, Si, Na, Ca and Mg in the unfiltered and filtered fresh and aged suspensions, the samples were acidified (HNO_3 (Merck, suprapure)) and diluted as required for analysis by inductively coupled plasma mass spectrometry (ICP-MS; Agilent 7500ce). The analysis of unfiltered initial solutions (after Fe(II) spike) and unfiltered final fresh and aged suspensions by ICP-MS indicated a high recovery of the spiked As(V) (>96% for 90% of the fresh suspensions; >94% for 90% of aged suspensions) (Fig. S1 in supporting data). In the Ca and Ca+Si electrolytes, we previously observed a decrease in P recovery from fresh to aged suspensions at the lowest and highest $(\text{P/Fe})_{\text{init}}$, which we attributed to co-precipitation of P with Ca-carbonates or precipitation of Ca-phosphate on the walls of the reaction vessels (Senn et al. 2017). Analogous effects appeared to be negligible for As(V).

The amounts of As, P and Fe in the precipitates (As_{ppt} , P_{ppt} , Fe_{ppt}) were calculated from their total concentration in the initial solution and the concentrations of As and P measured in the final filtered solutions (As_{filt} , P_{filt}). This calculation was based on the assumption that As_{filt} and P_{filt} corresponded to the dissolved concentrations As_{soln} and P_{soln} , respectively, and that the concentration of dissolved Fe_{soln} was negligible. In some of the filtered solutions from fresh and aged Na and Na+Si suspensions, however, measurable Fe concentrations indicated the presence of colloidal Fe. This observation was attributed to the stabilizing effects of P and Si on Fe(III)-colloids and the limited coagulating power of Na (Mayer and Jarrell 1996, Tessenow 1974) or to filter failure in two cases. To estimate the concentrations of colloidal As and P (As_{coll} , P_{coll}) in these electrolytes, it was assumed that the colloidal Fe-precipitates had the same As/Fe and P/Fe ratios as determined for the respective Fe(III)-precipitates

retained on the filter membranes and that the concentration of colloidal Fe corresponded to Fe_{filt} . The dissolved concentrations X_{soln} ($X=As$ or P) were calculated by subtracting X_{coll} from X_{filt} . This correction is further described in the supplementary data (Fig. S2). Because dissolved As and P concentrations in the fresh Na+Si electrolyte at $(P/Fe)_{\text{init}} \leq 0.4$ were too low for quantification, they were set to zero for data interpretation on a linear scale, and were omitted in plots on a logarithmic scale.

2.3. Model calculations

A kinetic adsorption/co-precipitation model has been formulated by (Roberts et al. 2004) to describe the removal of Si, P, As(V) and As(III) during Fe(II) oxidation and Fe(III) precipitation in aerated water. The model assumes that Si, P and As competitively bind on a single type of sorption site $\equiv Fe$ whose concentration $[\equiv Fe]$ is proportional to the total Fe(III) concentration $[Fe]_{\text{tot}}$:

$$[\equiv Fe] = S \times [Fe]_{\text{tot}} \quad (\text{Eq. 1})$$

S representing the number of sorption sites per Fe. At equilibrium, this kinetic model corresponds to a competitive Langmuir sorption model characterized by the site concentration $S \times [Fe]_{\text{tot}}$ and the sorption coefficients K_x for oxyanion uptake, where $[\equiv FeX]$ and $[X]$ denote the concentrations of the sorbed and dissolved oxyanion X:



$$K_x = \frac{[\equiv FeX]}{[\equiv Fe] \times [X]} \quad (\text{Eq. 3})$$

This model was used to describe residual dissolved As(V) and P in the fresh precipitate suspensions based on total initial concentrations of Fe, As(V), P and Si. For this purpose, the model was set up in PhreeqC (Parkhurst and Appelo 1999) within PhreePlot (Kinniburgh and Cooper 2016), and the non-linear least squares (modified Levenberg-Marquardt) procedure of PhreePlot was used to derive the parameters S and K_x and their statistical uncertainty. Further details on model calculations are provided in section 3.4.

3. RESULTS AND DISCUSSION

3.1. Dissolved As(V) concentrations in fresh suspensions

The dissolved fractions of As in the fresh suspensions as a function of $(P/Fe)_{init}$ for the six background electrolytes are shown in Figure 1, together with the data for P from (Senn et al. 2015). To facilitate the comparison of dissolved As fractions in the different fresh suspensions, the respective data are shown in an overlay plot in Figure 2a. To demonstrate major effects of $(P/Fe)_{init}$, Si and Ca on As(V) removal and release, selected treatments are compared in Figure 3. Whereas the initial dissolved As(V) concentration ($As(V)_{init}$) was 7 μM in all treatments, the P concentrations (P_{init}) varied from 0 to 1 mM. Despite this difference, the fractions of dissolved As and P generally show similar trends. Changes in precipitate structure and dissolved P as a function of $(P/Fe)_{init}$ and electrolyte type have been described in detail in earlier work (Senn et al. 2015) and are summarized in the introduction and in Table 1. Here, we focus on how dissolved As(V) was influenced by $(P/Fe)_{init}$ and by the absence or presence of Si and Ca.

At $(P/Fe)_{init}$ above $(P/Fe)_{crit}$ (Table 1), the oxyanion uptake capacity of amorphous (Ca-)Fe(III)-phosphate was exceeded and residual dissolved As(V) increased markedly with increasing $(P/Fe)_{init}$ (Figure 2a). Under these conditions, As(V) uptake did not depend on the absence or presence of Si, but a strong effect of the electrolyte cation was observed, with markedly higher removal in the Ca and Ca+Si electrolytes than in the Na and Na+Si electrolytes. This difference was due to the higher oxyanion uptake capacity of Ca-Fe(III)-phosphate as compared with Fe(III)-phosphate (Figure 1).

At intermediate $(P/Fe)_{init}$, Ca strongly influenced As(V) sequestration via its effect on the oxyanion uptake capacity of amorphous Ca-Fe(III)-phosphate and thus on $(P/Fe)_{crit}$. (Note: We refer to these precipitates as Ca-Fe(III)-phosphate rather than Ca-Fe(III)-phosphate/arsenate because P is the dominant oxyanion and As(V) is only coprecipitated at

molar As(V)/P ratios < 0.03 .) Below $(P/Fe)_{crit}$, the very low dissolved fractions of As(V) in the Si-containing electrolytes (Figure 1c,d, Figure 2a) reflected its highly effective sorption by Si-rich ferrihydrite, whose fraction increased with decreasing $(P/Fe)_{init}$. In the Si-free electrolytes, the fractions of residual dissolved As(V) increased as $(P/Fe)_{init}$ decreased from $(P/Fe)_{crit}$ to 0.05 (Figure 1a,e), as also observed for P (Figure 1b,f, Figure 2). This effect was attributed to the immediate onset of precipitate aging after Fe(II) oxidation at $(P/Fe)_{init} < (P/Fe)_{crit}$, as has previously been discussed for P (Mayer and Jarrell 2000, Senn et al. 2015, Voegelin et al. 2013) and As(V) (Fuller et al. 1993) release from Fe(III)-precipitates. In the Si-containing electrolytes, this effect was not observed (Figure 1c,d, Figure 2a) due to the inhibiting effects of Si (and Ca) on precipitate transformation combined with the efficient uptake of any released As(V) and P by ferrihydrite (and Ca-phosphate precipitation).

In general, residual dissolved As(V) and P fractions in fresh suspensions exhibited similar trends (Figure 1). To directly compare As(V) and P uptake by fresh precipitates as a function of $(P/Fe)_{init}$ and of Si and Ca in the electrolyte, molar precipitate As/P ratios relative to the corresponding initial dissolved ratios ($(As/P)_{ppt,rel} = (As/P)_{ppt}/(As/P)_{init}$) are shown in Figure 4 for the Na, Ca, Na+Si and Ca+Si electrolytes. At low $(P/Fe)_{init}$ in the Na and Ca electrolytes, uptake of As by poorly-crystalline lepidocrocite was slightly favored over P uptake. This effect was not observed in the Na+Si and Ca+Si electrolytes, where Si-rich ferrihydrite was the dominant precipitate. At intermediate $(P/Fe)_{init}$, $(As/P)_{ppt,rel}$ around unity indicated that As(V) and P were taken up to similar extents in all electrolytes. At $(P/Fe)_{init} > (P/Fe)_{crit}$ in the Na and Na+Si electrolytes, P exhibited a slight preference over As(V) for sequestration by Fe(III)-phosphate. The preference for P over As(V) was more pronounced for Ca-Fe(III)-phosphate formed in the Ca and Ca+Si electrolytes, which was attributed to specific Ca-P interactions, including the formation of Ca-Fe(III)-phosphate and Ca-phosphate polymers (Senn et al. 2015). More specific Ca-P than Ca-As(V) interactions can be

rationalized by the observation that Ca-phosphates exhibit much lower solubilities than structurally analogous Ca- arsenates (Voegelin et al. 2010) and the result from an adsorption study with goethite indicating a stronger enhancing effect of Ca on P than As(V) uptake (Gao and Mucci 2003).

3.2. Dissolved As(V) in aged precipitate suspensions

In Figure 5, the dissolved fractions of As and P in all aged electrolyte suspensions are shown in comparison to the fractions in the fresh suspensions. Dissolved fractions of As(V) in all aged suspensions are compared in an overlay plot in Figure 2b, the effects of P, Si, and Ca on the residual dissolved fraction of As in selected treatments are shown in Figure 3.

At high $(P/Fe)_{init}$ in the electrolytes without or with only 0.5 mM Ca (Na, Na+Si, Mg and low Ca electrolytes), the residual dissolved As(V) concentrations exhibited no significant changes from before to after aging (Figure 5a, e; Figure 3d). This was attributed to the stabilization of the precipitate towards Fe(III)-polymerization by the residual dissolved P in the aging suspension. In the presence of 4 mM total Ca (Ca, Ca+Si electrolytes), dissolved As(V) concentrations at high $(P/Fe)_{init}$ decreased during aging, and an even stronger decrease was observed for P (Figure 5c,d). The decrease in dissolved As(V) may be due to co-precipitation of As(V) with Ca-phosphate which formed during aging (Senn et al. 2017), but could also be due to uptake of As by Ca-Fe(III)-phosphate from which P may have been depleted by Ca-phosphate precipitation. In the low Ca electrolyte, no decrease of the dissolved As(V) was observed during aging (Figure 5f) because the dissolved Ca concentration was too low to induce the formation of a Ca-phosphate precipitate (Senn et al. 2017).

At intermediate $(P/Fe)_{init}$, the stabilizing effect of Ca on Ca-Fe(III)-phosphate resulted in a markedly lower remobilization of As during aging than in the Ca-free treatments (Figure 2),

especially at $(P/Fe)_{init}$ between the $(P/Fe)_{crit}$ of the Na and Ca electrolytes (e.g., $(P/Fe)_{init}$ of 0.6; Figure 3c).

At low $(P/Fe)_{init}$ in the Si-free electrolytes, aging led to substantial release of As(V) (Figure 2b, Figure 5a,e). Precipitate aging started immediately after Fe(II) oxidation was complete (Voegelin et al. 2013) and could already be detected in the fresh precipitate suspensions 4 h after Fe(II) addition (Senn et al. 2015) (Figure 2a). Again, the release of As(V) was most pronounced in the Na background electrolyte, where at $(P/Fe)_{init}$ between 0.1 and 0.2, the dissolved fraction of As increased from ~8% to ~55% (Figure 2). The stabilizing effect of Si ferrihydrite at low $(P/Fe)_{init}$ is reflected in the lower As remobilization in the Na+Si electrolyte than in the Na electrolyte (Figure 2, Figure 5a, b). An even lower release was observed in the Ca+Si electrolyte (Figure 2, Figure 5c), where Ca inhibited the transformation of Ca-Fe(III)-phosphate. In addition, Ca-phosphate precipitation may have attenuated the competition of any released As and P for sorption to Ca-Fe(III)-phosphate.

During aging, the pH of the suspensions increased from pH 7.0 to pH 7.9 ± 0.3 , due to CO₂ outgassing that was partially compensated by continuing Ca-carbonate precipitation in the Ca and Ca+Si electrolytes at low $(P/Fe)_{init}$ (Senn et al. 2017) as well as by the continuing Fe(III) polymerization, especially in the Na electrolyte at intermediate $(P/Fe)_{init}$. Considering that the adsorption of As(V) and P on pre-formed ferrihydrite decreases with increasing pH (Antelo et al. 2015, Dixit and Hering 2003), the increase in pH during aging may have contributed to drive As(V) and P release in some of the treatments. However, the extent of As(V) and P release in our experiments and trends in As(V) and P release as a function of $(P/Fe)_{init}$ and background electrolyte composition suggest that ongoing Fe(III) polymerization and Fe(III)-precipitate transformation were the main factors that caused As(V) and P release during aging.

3.3. Time-resolved aging experiment

To monitor the time-dependence of As(V) and P remobilization during aging, time resolved experiments were conducted at $(P/Fe)_{init}$ of 0.25 in Na, Na+Si, Ca and Ca+Si electrolyte (Fig. 6). The data show that the marked release of As(V) and P in the Na and Na+Si electrolytes proceeds within the first days after Fe(II) oxidation and approaches a plateau after 7-10 days. The pH increased from initially 7.0 to 7.8-8.2 after 35 days of aging, in line with pH values in aged suspensions from the multifactorial experiment (Senn et al. 2017).

Interestingly, the dissolved fractions of As(V) and P in the Ca electrolyte initially increased due to remobilization, but started to decrease again after ~21 and ~10 days, respectively. We attribute these trends to the precipitation of Ca-phosphate and Ca-carbonate (as indicated by trends in dissolved Ca) and co-precipitation of As(V) and P. In the Ca+Si electrolyte, the slow increase in dissolved As(V) and P may be due to concomitant oxyanion release from slowly transforming Fe(III)-precipitates and co-precipitation with Ca. The interplay between the aging of the Fe(III)-precipitates and related remobilization of As(V) and P and the concomitant formation of Ca-phases that may re-sequester released As(V) and P may have important environmental implications and warrants further study.

3.4. Modeling residual dissolved As(V) and P in fresh precipitate suspensions

In a study on the removal of As(III) and As(V) by co-oxidation and co-precipitation with Fe(II) in synthetic Bangladesh groundwater (SBGW), Roberts et al. (2004) developed a kinetic competitive oxyanion co-precipitation model to describe residual dissolved As concentrations. The same model was applied by Berg et al. (2006) to rationalize results from a study on As(III) and As(V) removal in sand filters in Vietnam. More recently, the same approach was implemented in a kinetic model to describe the removal of As(III) by electrocoagulation (Li et al. 2012). We used an equilibrium formulation of the same model

that corresponds to a one-site competitive Langmuir sorption model to describe residual dissolved As(V), P and Si in the fresh precipitate suspensions based on the initial total concentration of As(V), P, Si and Fe. Model parameters were optimized by minimizing the sum of the squared residuals between experimental and modeled concentrations of dissolved As(V) (multiplied by 100 to give weight similar to P and Si), P and Si. Because the model does not account for the incipient precipitate transformation and oxyanion release observed in the Si-free electrolytes at $(P/Fe)_{init} < 0.4$, the respective data was excluded from modeling.

Model parameters from a first fit with a single site capacity and a single set of sorption coefficients for all treatments were comparable to parameters reported by Roberts et al. (2004) (Table 2). In both studies, about 0.2 units higher $\log K_P$ than $\log K_{As}$ values indicated a slight preference for uptake of P over As(V), in line with $(As/P)_{ppt,rel} < 1$ at high $(P/Fe)_{init}$ reported in Figure 4. To account for the difference in the oxyanion uptake capacity of precipitates formed in the electrolytes with high Ca (Ca, Ca+Si), with low Ca or Mg, or no Ca or Mg (Na and Na+Si) and potential differences in oxyanion sorption affinity, the data from the respective sets of samples were also fit separately (Table 2; fitted As(V) and P fractions shown in Fig. 1). This approach allowed for a significantly more accurate description of the experimental data (decrease of SSR from 0.279 to 0.055). The much higher site concentration for the Ca / Ca+Si electrolytes than the Mg / low Ca electrolytes reflected the formation of Ca-phosphate and Ca-Fe(III)-phosphate polymers in the Ca and Ca+Si electrolytes. The sorption coefficients pointed to variations in the relative sorption affinities of As and P: Whereas no marked preference for P over As was observed for the Na / Na+Si and Mg / low Ca electrolytes, the presence of 4 mM Ca in the Ca / Ca+Si electrolytes resulted in a markedly higher difference between $\log K_P$ and $\log K_{As}$ that reflects the preference of Ca for complexation with P rather than As(V) (van Genuchten et al. 2014a). Since the enhanced uptake of P in the Ca / Ca+Si electrolytes is not solely due to co-precipitation with Fe(III),

but also due to precipitation of Ca-phosphate polymers, the sorption coefficient K_P must however be interpreted with care.

Because the model parameters were refined based on residual dissolved concentrations on a linear scale, the fits were mainly sensitive to treatments with high residual dissolved P and As(V) fractions, i.e., treatments at high $(P/Fe)_{init}$ in which (Ca-)Fe(III)-phosphate formed and As(V) and P sequestration occurred via co-precipitation rather than adsorption at the surface of an Fe(III)-(hydr)oxide. Although it might be more appropriate to describe these co-precipitates with a solubility product, such an approach is complicated by the fact that the phase composition and thus the solubility product itself depend on solution chemistry (Stumm et al. 1962, van der Grift et al. 2016). In a study on P removal from wastewater, variations in the $(P/Fe)_{ppt}$ of amorphous Fe(III)-phosphate were accounted for by modeling the precipitation of a Fe(III)-phosphate with $(P/Fe)_{ppt}$ of 0.4 combined with P adsorption to the Fe(III)-phosphate (Luedecke et al. 1989). In our sorption model, variations in the number of free adsorption sites provide some flexibility to account for variations in the oxyanion uptake of (Ca-)Fe(III)-phosphate as a function of $(P/Fe)_{init}$ and resulting variations in residual dissolved P and As(V).

At $(P/Fe)_{init} < (P/Fe)_{crit}$ in the Si-containing fresh electrolytes where Si-ferrihydrite was the dominant precipitate type and precipitate aging was still limited, measured dissolved As(V) and P fractions were close to 0% on a linear scale (Figure 1c,d). The model, on the other hand, predicted concentrations in the low percent range, overestimating the dissolved As(V) and P relative to measured concentrations. This suggests that As(V) and P sorption to ferrihydrite results in lower dissolved As(V) and P concentrations than expected for solubility control by (Ca-)Fe(III)-phosphate.

To obtain an adequate description of dissolved As(V) and P concentrations over wide ranges in solution concentrations on a logarithmic scale, a multi-component model

accounting for the formation of different phases with different sorption site concentration and sorption affinities would be required. In addition to oxyanion uptake by different Fe(III)-precipitate types and the influence of cations, such a kinetic model would also have to account for Fe(III)-precipitate transformation processes and concomitant oxyanion release, Ca-phosphate and Ca-carbonate precipitation, and related As(V) and P re-precipitation.

3.5. Comparison of residual dissolved As(V) and P fractions with previous studies

In Figure 7, the residual fractions of As(V) and P from the fresh Na+Si and Ca+Si suspensions are shown together with data from Roberts et al. (2004). This study examined the removal of 6.7 μ M As(V) or As(III) from synthetic Bangladesh groundwater with constant Si and P (2.5 mM Ca; 1.5 mM Mg; 1.07 mM Si; 0.097 mM P; pH \sim 7) as a function of single additions of 0.9 to 0.04 mM Fe(II) (corresponding to increasing $(P/Fe)_{init}$). At $(P/Fe)_{init}$ of \sim 0.2, initial dissolved P and Fe(II) concentrations in the present work and in Roberts et al. (2004) as well as the respective $(As(V)/Fe)_{init}$ were similar, but the $(Si/Fe)_{init}$ in the current study (1.0) was lower than the $(Si/Fe)_{init}$ of \sim 2.2 in Roberts et al. (2004). In the present study, $(P/Fe)_{init}$ up to \sim 2 at constant $(Si/Fe)_{init}$ of 1.0 and $(As(V)/Fe)_{init}$ of 0.014 were obtained by increasing initial P_{diss} up to 1 mM. In contrast, Roberts et al. (2004) achieved an increase in $(P/Fe)_{init}$ up to 2.3 by decreasing the amount of spiked Fe(II) down to 0.04 mM, which resulted in a concomitant increase of $(Si/Fe)_{init}$ up to 25 and $(As(V)/Fe)_{init}$ or $(As(III)/Fe)_{init}$ up to 0.16 (Table S1). Despite these experimental differences, trends in residual dissolved As(V) and P fractions reported by Roberts et al. (2004) as a function of $(P/Fe)_{init}$ fall between the trends observed for the Na+Si and Ca+Si electrolytes (Figure 7), suggesting that the $(P/Fe)_{init}$ ratio is suitable to compare results obtained over a range in P and Fe concentrations.

Although the synthetic groundwater used by Roberts et al. (2004) contained 2.5 mM Ca, dissolved As(V) and P concentrations are more similar to the values from the Na+Si (with no Ca) than the Ca+Si treatment (with 4 mM Ca), suggesting that specific Ca-phosphate

interactions were less relevant than in the Ca+Si electrolyte. This difference can be explained by the increase of P_{init} up to 1 mM in the Ca+Si electrolyte, as compared to a constant P_{init} of ~ 0.097 in the experiments of Roberts et al. (2004), which corresponds to a much higher saturation index for Ca-phosphates in the current work than in Roberts et al. (2004). This interpretation is in line with the finding that the extent of P precipitation during groundwater aeration also depends on the degree of Ca-phosphate supersaturation (Griffioen 2006). Furthermore, the groundwater used by Roberts et al. (2004) contained 1.6 mM Mg that may inhibit the precipitation of Ca-phosphate (Brown 1981).

The comparison of the residual dissolved As in experiments with As(III) and As(V) from Roberts et al. (2004) illustrates the much lower affinity of As(III) than As(V) for coprecipitation during Fe oxidation and precipitation (Figure 7). Residual As and P fractions from a study on As(III) removal from synthetic groundwater by electrocoagulation (Li et al. 2012) are shown in Figure 7 for comparison as well (6.7 μ M As(III); 0.097 mM P, 1.07 mM Si, 2.5 mM $CaCl_2$, 1.6 mM $MgCl_2$, 8.2 mM $NaHCO_3$, pH 7.2). In this study, 0.6 to 0.06 mM Fe(II) were added at a rate of 0.016 mM/min through electrolytic dissolution of elemental Fe, corresponding to $(P/Fe)_{init}$ from ~ 0.16 to ~ 1.5 . The respective data for residual dissolved P closely match with data from Roberts et al. (2004), but the data for residual As point to more effective removal by continuous Fe(II) addition. This can be attributed to the slow release of Fe(II) during electrocoagulation, which leads to the formation of solids with higher oxyanion/Fe ratios and to more effective oxidation of As(III) to As(V) (Li et al. 2012), in line with observations by Roberts et al. (2004) for incremental versus single Fe(II) additions.

3.6. Environmental implications

This study showed how variations in solution chemistry affect As(V) sequestration by fresh Fe(III)-precipitates and how precipitate transformation during aging promotes As(V) resolubilization. In Figure 2cd, the concentrations of dissolved As(V) in fresh and aged

suspensions are shown on a logarithmic scale to visualize the main effects of $(P/Fe)_{init}$, Ca and Si on As(V) sequestration by fresh and aged precipitates and for comparison with drinking water guideline values. By inducing the formation of ferrihydrite that is stabilized against further polymerization (Mayer and Jarrell 2000, Senn et al. 2015, Senn et al. 2017, Voegelin et al. 2010), the presence of Si markedly reduces residual As(V) concentration at low $(P/Fe)_{init}$ to values below the WHO guideline value of 10 $\mu\text{g/L}$ (indicated by green arrow in Figure 2c). The impact of Ca is of particular importance at intermediate $(P/Fe)_{init}$, as it enhances the oxyanion uptake of the Fe(III)-precipitates through favorable electrostatic interactions, specific Ca-P interactions and by stabilizing the precipitates, especially Ca-Fe(III)-phosphate, against transformation. In natural waters, however, the effect of Ca may be smaller than observed in this study, because Ca and P concentrations are often lower and Mg or other solutes may inhibit Ca-phosphate precipitation.

Compared to average and median concentrations of Fe (3.4 and 1.1 mg/L; $n \sim 3500$) and P (0.7 and 0.3 mg/L) in groundwaters from Bangladesh, the Fe (28 mg/L) and P (0.7-31 mg/L) concentrations in our experiments were rather high. The median and 5-95 percentile range of the P/Fe ratio (0.25 and 0.02-5) of these groundwaters, on the other hand, which is of critical importance in As removal (Hug et al. 2008), relatively closely matched the range of $(P/Fe)_{init}$ (0-2) probed in our experiments. Compared to the $(Si/Fe)_{init}$ of 1.0 in the Na+Si and Ca+Si electrolytes, the Si/Fe ratios of Bangladesh groundwaters tend to be much higher (minimum 0.8, median 35). The average concentration of Ca (52 mg/L) in Bangladesh groundwaters lies between the Ca concentrations in the Ca / Ca+Si electrolytes (160 mg/L Ca) and the low Ca electrolyte (20 mg/L). Thus, based on typical concentrations of Fe, P, Si and Ca in anoxic As-containing groundwaters from Bangladesh (BGS and DPHE 2001), Vietnam and Cambodia (Hug et al. 2008), precipitates formed during groundwater oxygenation are expected to range from Si-rich ferrihydrite to Ca-containing Fe(III)-

phosphate, and results from the low Ca and Ca+Si electrolytes are most directly applicable to infer the extent of As(V) sequestration by fresh and aged precipitates in field systems.

High P/Fe ratios that are frequently found in Bengali groundwaters pose special difficulties for As removal (Hug et al. 2008) and require techniques that involve the addition of supplementary Fe, either as dissolved Fe(II) (Meng et al. 2001, Roberts et al. 2004), through corrosion of zerovalent iron (ZVI) (Leupin et al. 2005, Su and Puls 2001a) or via and electrocoagulation (Lakshmanan et al. 2009, Li et al. 2012, Ratna Kumar et al. 2004). With respect to such systems, the Fe(II) concentration of 0.5 mM used in the present study falls well into the technically relevant range.

During the aging of the precipitate suspensions for 30 days at 40°C, dissolved As(V) concentrations in (nearly) all treatments remained stable or increased to levels above the WHO guideline value (Figure 2d). Nevertheless, at intermediate and low (P/Fe)_{init}, Ca and Si exhibited markedly inhibited precipitate transformation and As(V) release. However, both Ca and Si were required to prevent As(V) re-solubilization to levels above the Bengali drinking water guideline value of 50 µg/L. With respect to the operation of drinking water treatment systems for As removal and the handling of treatment residues, our data show that fresh Fe(III)-precipitates may effectively reduce dissolved As, but that transformation of fresh precipitates to more polymerized or crystalline solids with lower oxyanion sorption capacity may result in substantial release of temporarily retained As within a time period of a few days to few weeks. On the other hand, the results also point to the importance of Ca-precipitate formation for longer-term As(V) retention.

The results from this study are not only of importance with respect to Fe-based As(V) removal from drinking water, but also contribute to a better understanding of As dynamics in agricultural fields and especially rice paddies irrigated with As-rich groundwater. In these systems, Fe(III)-precipitate formation and transformation not only impact the introduction of

As into the soils (Dittmar et al. 2007, Roberts et al. 2007), but also As accumulation around rice roots (Frommer et al. 2011) as well as As accumulation in soils and release during monsoon flooding (Dittmar et al. 2010b, Roberts et al. 2010).

4. CONCLUSIONS

This study reveals how Si, P and Ca, via their effects on Fe(III)-precipitate structure and ion co-sorption, critically influence the uptake of As(V) by fresh and aged Fe(III)-precipitates. Variations in the extent of As(V) sequestration can be rationalized in terms of competitive oxyanion uptake and the structural diversity of the precipitating Fe(III)-solids. The results highlight the important roles of Ca and Si in promoting As(V) removal by fresh precipitates and As(V) retention during precipitate aging and indicate that results from studies in simplified Na-electrolytes must be considered with care with respect to their transferability to natural waters containing Ca and Si.

A simple single-phase sorption model is adequate to describe residual dissolved As(V) in fresh suspensions under conditions where saturation of the oxyanion uptake capacity limits removal. To describe the solubility of As(V) and other oxyanions under conditions where the sorption capacity of the Fe(III)-precipitates is not reached, a more complex kinetic modeling approach would be required that accounts for the structural diversity of fresh precipitates, their transformation over time, and the concomitant formation of Ca-phases.

5. ACKNOWLEDGEMENTS

Irene Brunner, Thomas Rüttimann and Numa Pfenninger (Eawag, Switzerland) are acknowledged for assistance with laboratory experiments and analyses. This project was financially supported by the Swiss National Science Foundation under contracts No. 200021-132123 and 200020-152993.

- Antelo, J., Arce, F. and Fiol, S. (2015) Arsenate and phosphate adsorption on ferrihydrite nanoparticles. Synergistic interaction with calcium ions. *Chemical Geology* 410, 53-62.
- Bang, S., Korfiatis, G.P. and Meng, X. (2005) Removal of arsenic from water by zero-valent iron. *Journal of Hazardous Materials* 121(1-3), 61-67.
- Berg, M., Luzi, S., Trang, P.T.K., Viet, P.H. and Giger, W. (2006) Arsenic removal from groundwater by household sand filters: Comparative field study, model calculations, and health benefits. *Environmental Science and Technology* 40, 5567-5573.
- BGS and DPHE (2001) Arsenic contamination of groundwater in Bangladesh. Kinniburgh, D.G. and Smedley, P.L. (eds), British Geological Survey (BGS) & Bangladesh Department for Public Health Engineering (DPHE), Keyworth, UK.
- Brown, J.L. (1981) Calcium phosphate precipitation: Effects of common and foreign ions on hydroxyapatite crystal growth. *Soil Science Society of America Journal* 45, 482-486.
- Chen, N., Jiang, D.T., Cutler, J., Kotzer, T., Jia, Y.F., Demopoulos, G.P. and Rowson, J.W. (2009) Structural characterization of poorly-crystalline scorodite, iron(III)-arsenate coprecipitates and uranium mill neutralized raffinate solids using X-ray absorption fine structure spectroscopy. *Geochimica et Cosmochimica Acta* 73, 3260-3276.
- Delaire, C., Amrose, S., Zhang, M., Hake, J. and Gadgil, A. (2017) How do operating conditions affect As(III) removal by iron electrocoagulation? *Water Research* 112, 185-194.
- Dittmar, J., Voegelin, A., Maurer, F., Roberts, L.C., Hug, S.J., Saha, G.C., Ali, M.A., Badruzzaman, A.B.M. and Kretzschmar, R. (2010a) Arsenic in soil and irrigation water affects arsenic uptake by rice: Complementary insights from field and pot studies. *Environmental Science and Technology* 44, 8842-8848.
- Dittmar, J., Voegelin, A., Roberts, L.C., Hug, S.J., Saha, G.C., Ali, M.A., Badruzzaman, A.B.M. and Kretzschmar, R. (2007) Spatial distribution and temporal variability of arsenic in irrigated rice fields in Bangladesh: 2. Paddy soil. *Environmental Science and Technology* 41, 5967-5972.
- Dittmar, J., Voegelin, A., Roberts, L.C., Hug, S.J., Saha, G.C., Ali, M.A., Badruzzaman, A.B.M. and Kretzschmar, R. (2010b) Arsenic accumulation in a paddy field in Bangladesh: Seasonal dynamics and trends over a three-year monitoring period. *Environmental Science and Technology* 44, 2925-2931.
- Dixit, S. and Hering, J.G. (2003) Comparison of arsenic(V) and arsenic(III) sorption onto iron oxide minerals: Implications for arsenic mobility. *Environmental Science and Technology* 37, 4182-4189.
- Ford, R.G. (2002) Rates of hydrous ferric oxide crystallization and the influence on coprecipitated arsenic. *Environmental Science and Technology* 36, 2459-2463.
- Frommer, J., Voegelin, A., Dittmar, J., Marcus, M.A. and Kretzschmar, R. (2011) Biogeochemical processes and arsenic enrichment around rice roots in paddy soil: results from micro-focused X-ray spectroscopy. *European Journal of Soil Science* 62, 305-317.
- Fuller, C.C., Davis, J.A. and Waychunas, G.A. (1993) Surface chemistry of ferrihydrite: Part 2. Kinetics of arsenate adsorption and coprecipitation. *Geochimica et Cosmochimica Acta* 57, 2271-2282.
- Gao, Y. and Mucci, A. (2003) Individual and competitive adsorption of phosphate and arsenate on goethite in artificial seawater. *Chemical Geology* 199, 91-109.

558 Griffioen, J. (2006) Extent of immobilisation of phosphate during aeration of nutrient-rich,
559 anoxic groundwater. *Journal of Hydrology* 320, 359-369.

560 Hug, S.J. and Leupin, O. (2003) Iron-catalyzed oxidation of arsenic(III) by oxygen and by
561 hydrogen peroxide: pH-dependent formation of oxidants in the Fenton reaction.
562 *Environmental Science and Technology* 37, 2734-2742.

563 Hug, S.J., Leupin, O.X. and Berg, M. (2008) Bangladesh and Vietnam: Different
564 groundwater compositions require different approaches to arsenic mitigation.
565 *Environmental Science and Technology* 42, 6318-6323.

566 Katsoyiannis, I.A., Ruettimann, T. and Hug, S.J. (2008) pH dependence of Fenton reagent
567 generation and As(III) oxidation and removal by corrosion of zero valent iron in aerated
568 water. *Environmental Science and Technology* 42, 7424-7430.

569 Kinniburgh, D.G. and Cooper, D.M. (2016) PhreePlot: Creating graphical output with
570 PHREEQC.

571 Lakshmanan, D., Clifford, D.A. and Samanta, G. (2009) Ferrous and ferric ion generation
572 during iron electrocoagulation. *Environmental Science and Technology* 43(10), 3853-
573 3859.

574 Leupin, O.X. and Hug, S.J. (2005) Oxidation and removal of arsenic(III) from aerated
575 groundwater by filtration through sand and zero-valent iron. *Water Research* 39, 1729-
576 1740.

577 Leupin, O.X., Hug, S.J. and Badruzzaman, A.B.M. (2005) Arsenic removal from Bangladesh
578 tube well water with filter columns containing zerovalent iron filings and sand.
579 *Environmental Science and Technology* 39(20), 8032-8037.

580 Li, L., van Genuchten, C.M., Addy, S.E.A., Yao, J., Gao, N. and Gadgil, A.J. (2012)
581 Modeling As(III) oxidation and removal with iron electrocoagulation in groundwater.
582 *Environmental Science and Technology* 46, 12038-12045.

583 Luedecke, C., Hermanowicz, S.W. and Jenkins, D. (1989) Precipitation of ferric phosphate in
584 activated Sludge: A chemical model and its verification. *Water Science and Technology*
585 21(4-5), 325-337.

586 Majzlan, J., Lalinská, B., Chovan, M., Jurkovic, L., Milovská, S. and Göttlicher, J. (2007)
587 The formation, structure, and aging of As-rich hydrous ferric oxide at the abandoned Sb
588 deposit Pezinok (Slovakia). *Geochimica et Cosmochimica Acta* 71, 4206-4220.

589 Mayer, D.T. and Jarrell, W.M. (1996) Formation and stability of iron(II) oxidation products
590 under natural concentrations of dissolved silica. *Water Research* 30, 1208-1214.

591 Mayer, D.T. and Jarrell, W.M. (2000) Phosphorus sorption during iron(II) oxidation in the
592 presence of dissolved silica. *Water Research* 34, 3949-3956.

593 Melkonian, S., Argos, M., Hall, M.N., Chen, Y., Parvez, F., Pierce, B., Cao, H., Aschebrook-
594 Kilfoy, B., Ahmed, A., Islam, T., Slavcovich, V., Gamble, M., Haris, P.I., Graziano, J.H.
595 and Ahsan, H. (2013) Urinary and dietary analysis of 18,470 bangladeshis reveal a
596 correlation of rice consumption with arsenic exposure and toxicity. *PLoS One* 8(11),
597 e80691.

598 Meng, X., Bang, S. and Korfiatis, G.P. (2000) Effects of silicate, sulfate, and carbonate on
599 arsenic removal by ferric chloride. *Water Research* 34, 1255-1261.

600 Meng, X., Korfiatis, G.P., Christodoulatos, C. and Bang, S. (2001) Treatment of arsenic in
601 Bangladesh well water using a household co-precipitation and filtration system. *Water*
602 *Research* 35, 2805-2810.

603 Meng, X.G., Korfiatis, G.P., Bang, S.B. and Bang, K.W. (2002) Combined effects of anions
604 on arsenic removal by iron hydroxides. *Toxicology Letters* 133(1), 103-111.

605 Murcott, S. (2012) *Arsenic Contamination in the World - An International Sourcebook*, IWA
606 Publishing, London.

607 Nikolaidis, N.P., Dobbs, G.M. and Lackovic, J.A. (2003) Arsenic removal by zero-valent
608 iron: field, laboratory and modeling studies. *Water Research* 37(6), 1417-1425.

609 Paktunc, D., Dutrizac, J. and Gertsman, V. (2008) Synthesis and phase transformations
610 involving scorodite, ferric arsenate and arsenical ferrihydrite: Implications for arsenic
611 mobility. *Geochimica et Cosmochimica Acta* 72, 2649-2672.

612 Paktunc, D., Majzlan, J., Huang, A., Thibault, Y., Johnson Michel, B. and White Mary, A.
613 (2015) Synthesis, characterization, and thermodynamics of arsenates forming in the Ca-
614 Fe(III)-As(V)-NO₃ system: Implications for the stability of Ca-Fe arsenates, p. 1803.

615 Panaullah, G.M., Alam, T., Hossain, M.B., Loeppert, R.H., Lauren, J.G., Meisner, C.A.,
616 Ahmed, Z.U. and Duxbury, J.M. (2008) Arsenic toxicity to rice (*Oryza sativa* L.) in
617 Bangladesh. *Plant and Soil* 317(1), 31.

618 Parkhurst, D.L. and Appelo, C.A.J. (1999) User's guide to PHREEQC (Version 2) -- a
619 computer program for speciation, batch-reaction, one-dimensional transport, and inverse
620 geochemical calculations, p. 312, U.S. Geological Survey, Denver, CO.

621 Ratna Kumar, P., Chaudhari, S., Khilar, K.C. and Mahajan, S.P. (2004) Removal of arsenic
622 from water by electrocoagulation. *Chemosphere* 55(9), 1245-1252.

623 Roberts, L.C., Hug, S.J., Dittmar, J., Voegelin, A., Kretzschmar, R., Wehrli, B., Cirpka, O.A.,
624 Saha, G.C., Ali, M.A. and Badruzzaman, A.B.M. (2010) Arsenic release from paddy
625 soils during monsoon flooding. *Nature Geoscience* 3, 53-59.

626 Roberts, L.C., Hug, S.J., Dittmar, J., Voegelin, A., Saha, G.C., Ali, M.A., Badruzzaman,
627 A.B.M. and Kretzschmar, R. (2007) Spatial distribution and temporal variability of
628 arsenic in irrigated rice fields in Bangladesh: 1. Irrigation water. *Environmental Science*
629 *and Technology* 41, 5960-5966.

630 Roberts, L.C., Hug, S.J., Ruettimann, T., Billah, M.M., Khan, A.W. and Rahman, M.T.
631 (2004) Arsenic removal with iron(II) and iron(III) in waters with high silicate and
632 phosphate concentrations. *Environmental Science and Technology* 38, 307-315.

633 Senn, A.-C., Kaegi, R., Hug, S.J., Hering, J.G., Mangold, S. and Voegelin, A. (2015)
634 Composition and structure of Fe(III)-precipitates formed by Fe(II) oxidation in near-
635 neutral water: Interdependent effects of phosphate, silicate and Ca. *Geochimica et*
636 *Cosmochimica Acta* 162, 220-246.

637 Senn, A.-C., Kaegi, R., Hug, S.J., Hering, J.G. and Voegelin, A. (2017) Effect of aging on the
638 structure and phosphate retention of Fe(III)-precipitates formed by Fe(II) oxidation in
639 water. *Geochimica et Cosmochimica Acta* 202, 341-360.

640 Smedley, P.L. and Kinniburgh, D.G. (2002) A review of the source, behaviour and
641 distribution of arsenic in natural waters. *Applied Geochemistry* 17, 517-568.

642 Stumm, W., Morgan, J.J. and Black, A.P. (1962) Chemical Aspects of Coagulation [with
643 Discussion]. *Journal (American Water Works Association)* 54(8), 971-994.

644 Su, C. and Puls, R.W. (2001a) Arsenate and arsenite removal by zerovalent iron: Effects of
645 phosphate, silicate, carbonate, borate, sulfate, chromate, molybdate, and nitrate, relative
646 to chloride. *Environmental Science and Technology* 35, 4562-4568.

- Su, C. and Puls, R.W. (2001b) Arsenate and arsenite removal by zerovalent iron: Kinetics, redox transformation, and implications for in situ groundwater remediation. *Environmental Science and Technology* 35, 1487-1492.
- Tessenow, U. (1974) Lösungs-, Diffusions- und Sorptionsprozesse in der Oberschicht von Seesedimenten. IV. Reaktionsmechanismen und Gleichgewichte im System Eisen-Mangan-Phosphat im Hinblick auf die Vivianitakkumulation im Ursee. *Archiv für Hydrobiologie Supplement* 47, 1-79.
- van der Grift, B., Behrends, T., Osté, L.A., Schot, P.P., Wassen, M.J. and Griffioen, J. (2016) Fe hydroxyphosphate precipitation and Fe(II) oxidation kinetics upon aeration of Fe(II) and phosphate-containing synthetic and natural solutions. *Geochimica et Cosmochimica Acta* 186, 71-90.
- van Genuchten, C.M., Addy, S.E.A., Pena, J. and Gadgil, A.J. (2012) Removing arsenic from synthetic groundwater with iron electrocoagulation: An Fe and As K-edge EXAFS study. *Environmental Science and Technology* 46, 986-994.
- van Genuchten, C.M., Gadgil, A.J. and Peña, J. (2014a) Fe(III) nucleation in the presence of bivalent cations and oxyanions leads to subnanoscale 7 Å polymers. *Environmental Science and Technology* 48, 11828-11836.
- van Genuchten, C.M., Peña, J., Amrose, S.E. and Gadgil, A.J. (2014b) Structure of Fe(III) precipitates generated by the electrolytic dissolution of Fe(0) in the presence of groundwater ions. *Geochimica et Cosmochimica Acta* 127, 285-304.
- Violante, A., Del Gaudio, S., Pigna, M., Ricciardella, M. and Banerjee, D. (2007) Coprecipitation of arsenate with metal oxides. 2. Nature, mineralogy, and reactivity of iron(III) precipitates. *Environmental Science and Technology* 41, 8275-8280.
- Voegelin, A., Kaegi, R., Frommer, J., Vantelon, D. and Hug, S.J. (2010) Effect of phosphate, silicate, and Ca on Fe(III)-precipitates formed in aerated Fe(II)- and As(III)-containing water studied by X-ray absorption spectroscopy. *Geochimica et Cosmochimica Acta* 74, 164-186.
- Voegelin, A., Senn, A.-C., Kaegi, R., Hug, S.J. and Mangold, S. (2013) Dynamic Fe-precipitate formation induced by Fe(II) oxidation in aerated phosphate-containing water. *Geochimica et Cosmochimica Acta* 117, 216-231.
- Waychunas, G.A., Rea, B.A., Fuller, C.C. and Davis, J.A. (1993) Surface chemistry of ferrihydrite: Part 1. EXAFS studies of the geometry of coprecipitated and adsorbed arsenate. *Geochimica et Cosmochimica Acta* 57, 2251-2269.
- Weber, F.-A., Hofacker, A., Voegelin, A. and Kretzschmar, R. (2010) Temperature dependence and coupling of iron and arsenic reduction and release during flooding of a contaminated soil. *Environmental Science and Technology* 44, 116-122.
- Wilkie, J.A. and Hering, J.G. (1996) Adsorption of arsenic onto hydrous ferric oxide: Effects of adsorbate/adsorbent ratios and co-occurring solutes. *Colloids and Surfaces A: Physicochemical and Engineering Aspects* 107, 97-110.

688 **Table 1.** Overview over the formation and structure of fresh Fe(III)-precipitates in Na,
 689 Na+Si, Ca, and Ca+Si electrolytes and corresponding critical P/Fe $((P/Fe)_{crit})^a$ (Senn et al.
 690 2015) and over changes in precipitate structure after aging for 30 d at 40 °C (Senn et al.
 691 2017).

Structure of fresh precipitates			
Electrolyte	$(P/Fe)_{crit}^a$	above $(P/Fe)_{crit}$	below $(P/Fe)_{crit}$
general		- exclusive precipitation of (Ca-)Fe(III)-phosphate - structural effect of Ca	- sequential precipitate formation, - first (Ca-)Fe(III)-phosphate until P depletion - subsequently structural effect of Si
Na	0.52 ± 0.01	- Fe(III)-phosphate	- Fe(III)-phosphate (<i>readily transforming</i>) - P-rich ferrihydrite - poorly-crystalline lepidocrocite
Na+Si	0.53 ± 0.01	- Fe(III)-phosphate	- Fe(III)-phosphate (<i>transforming</i>) - Si-rich ferrihydrite
Ca	0.85 ± 0.03	- Ca-Fe(III)-phosphate	- Ca-Fe(III)-phosphate (<i>Ca-stabilized</i>) - P-rich ferrihydrite - poorly-crystalline lepidocrocite
Ca+Si	0.87 ± 0.03	- Ca-Fe(III)-phosphate	- Ca-Fe(III)-phosphate (<i>Ca-stabilized</i>) - Si-rich ferrihydrite
Effects of aging on precipitate structure			
Electrolyte	above $(P/Fe)_{init} > 0.75$		below $(P/Fe)_{init} < 0.75$
general	- transformation inhibited by dissolved P and structural Ca		- transformation of (Ca-)Fe(III)-phosphate - Ca inhibits Ca-Fe(III)-phosphate transformation - Si inhibits ferrihydrite transformation
Na	- Fe(III)-phosphate		- Fe(III)-phosphate (<i>residual</i>) - P-rich ferrihydrite (<i>from Fe(III)-phosphate</i>) - poorly-crystalline lepidocrocite
Na+Si	- Fe(III)-phosphate		- Fe(III)-phosphate (<i>residual</i>) - Si- and P-containing ferrihydrite
Ca	- Ca-Fe(III)-phosphate		- Ca-Fe(III)-phosphate (<i>Ca-stabilized</i>) - (<i>P-rich ferrihydrite from Ca-Fe(III)-phosphate</i>) - poorly crystalline lepidocrocite
Ca+Si	- Ca-Fe(III)-phosphate		- Ca-Fe(III)-phosphate (<i>Ca-stabilized</i>) - Si-rich ferrihydrite-type precipitate

692 ^aThe critical P/Fe $((P/Fe)_{crit})$ refers to the initial dissolved P/Fe ratio $((P/Fe)_{init})$ above which
 693 exclusive formation of amorphous (Ca-)Fe(III)-phosphate occurs. At $(P/Fe)_{init} \sim (P/Fe)_{crit}$, the
 694 molar P/Fe ratio of the Fe(III)-precipitate $((P/Fe)_{ppt})$ corresponds to $\sim (P/Fe)_{init}$ (Senn et al.
 695 2015).

697 **Table 2.** Parameters of competitive co-precipitation model.^a

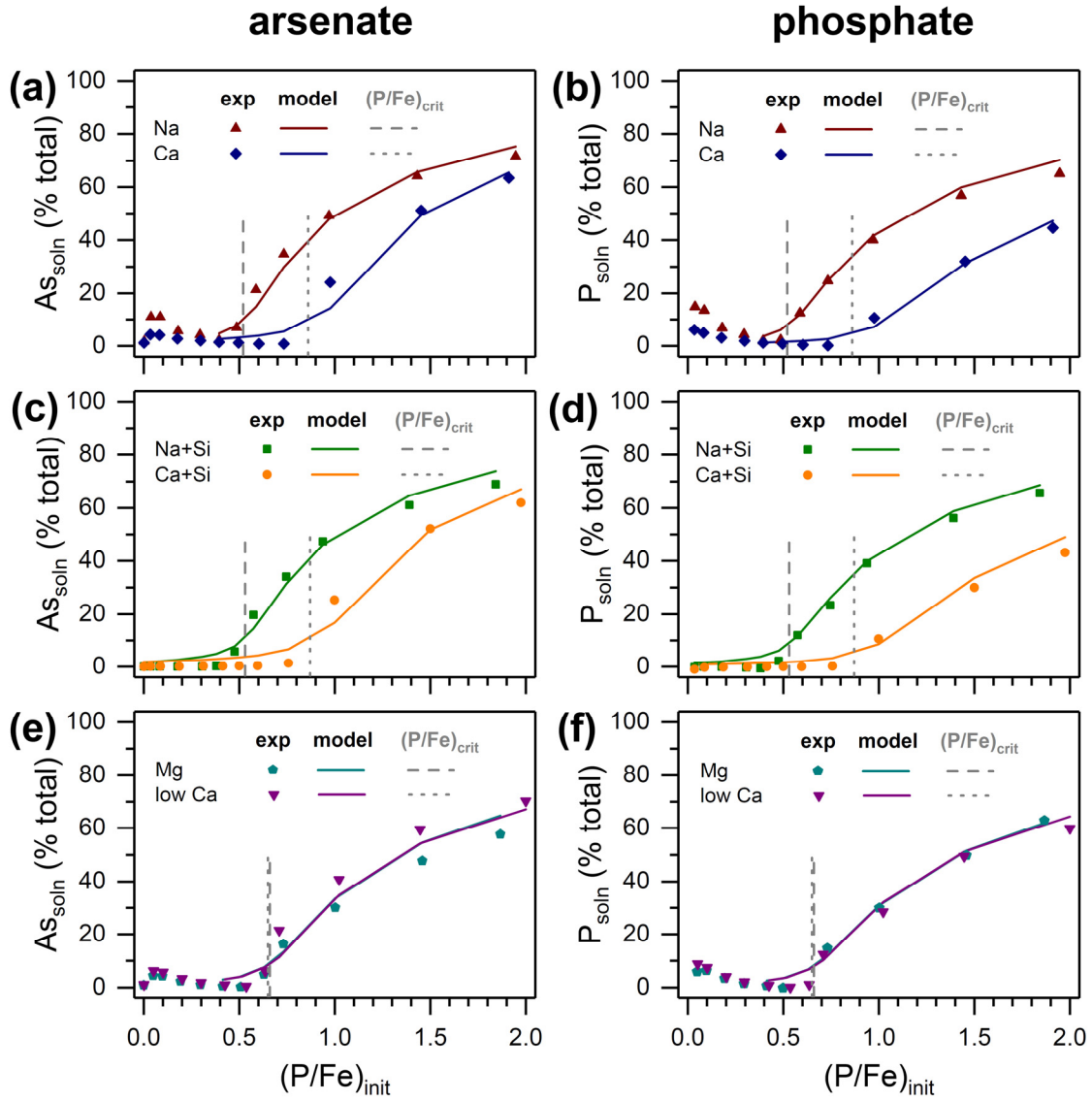
Electrolyte / Study	<i>S</i>	logK _{As}	logK _P	logK _{Si}	SSR
Na / Na+Si	0.58 (0.02)	5.34 (0.12)	5.45 (0.12)	2.46 (0.19)	0.055
Mg / low Ca	0.72 (0.02)	5.34 (0.14)	5.40 (0.13)	---	
Ca / Ca+Si	1.02 (0.02)	5.09 (0.10)	5.42 (0.10)	2.40 (0.11)	
All electrolytes	0.78 (0.03)	5.09 (0.12)	5.26 (0.12)	2.41 (0.22)	0.279
Roberts et al. (2004) ^b	0.72 (0.06)	5.72 (0.23)	5.87 (0.15)	2.77 (0.08)	---

698 ^aFit parameters obtained by non-linear least-squares minimization of the sum of the squared
699 residuals between modelled and measured concentrations of As(V) (weighed by factor 100),
700 P and Si in indicated electrolytes. For the Si-free electrolytes, the 5 datapoints from (P/Fe)_{init}
701 of 0 to 0.3 were not included, as the model does not account for As(V) and P release due to
702 continuing precipitate polymerization. *S* represents the site concentration in mole sites per
703 mole Fe, K_X represent the sorption coefficients for oxyanion X. Values in parentheses
704 indicate the estimated standard error.

705 ^bFit parameters from Roberts et al. (2004) for Fe(III)-precipitates formed by oxidation of
706 spiked Fe(II) (from fit with unconstrained parameters for As(III) co-oxidation; note that no
707 As(III) was used in current study).

708 ^cSSR = sum of squared residuals; Sum of SSR for Na/Na+Si, Ca/Ca+Si and Mg/low Ca
709 electrolytes (0.055) about 5 times lower than SSR of fit over all electrolytes.

710



711

712 Figure 1. Dissolved As (a,c,e) and P (b,d,f) fractions in fresh suspensions in percent of
 713 initially spiked amounts as a function of $(P/Fe)_{init}$ in Na, Ca, Na+Si, Ca+Si, low Ca and Mg
 714 background electrolytes. Thin vertical lines indicate the $(P/Fe)_{crit}$ of the respective
 715 electrolytes (from Senn et al. (2015)). Solid lines represent model calculations based on
 716 parameters optimized separately for the Na / Na+Si, the Ca / Ca+Si, and the Mg / low Ca
 717 electrolytes (Table 2). Data for dissolved P from Senn et al. (2015).

718

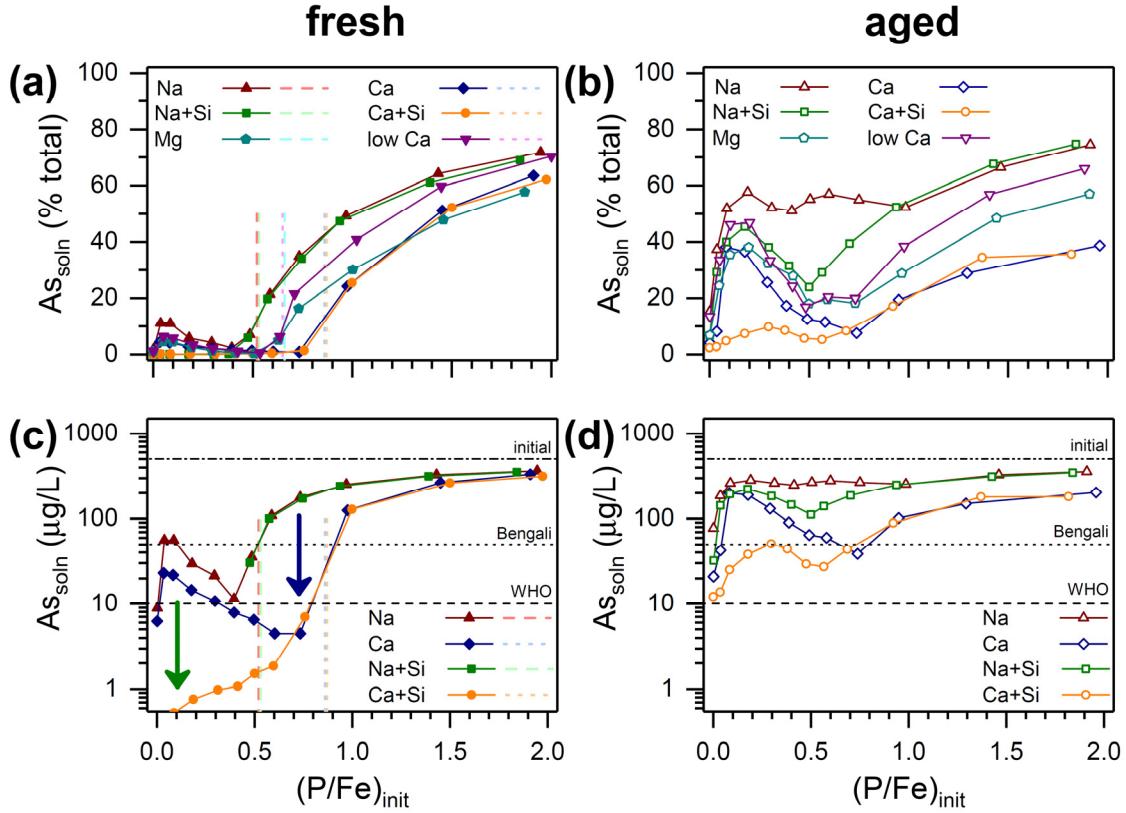
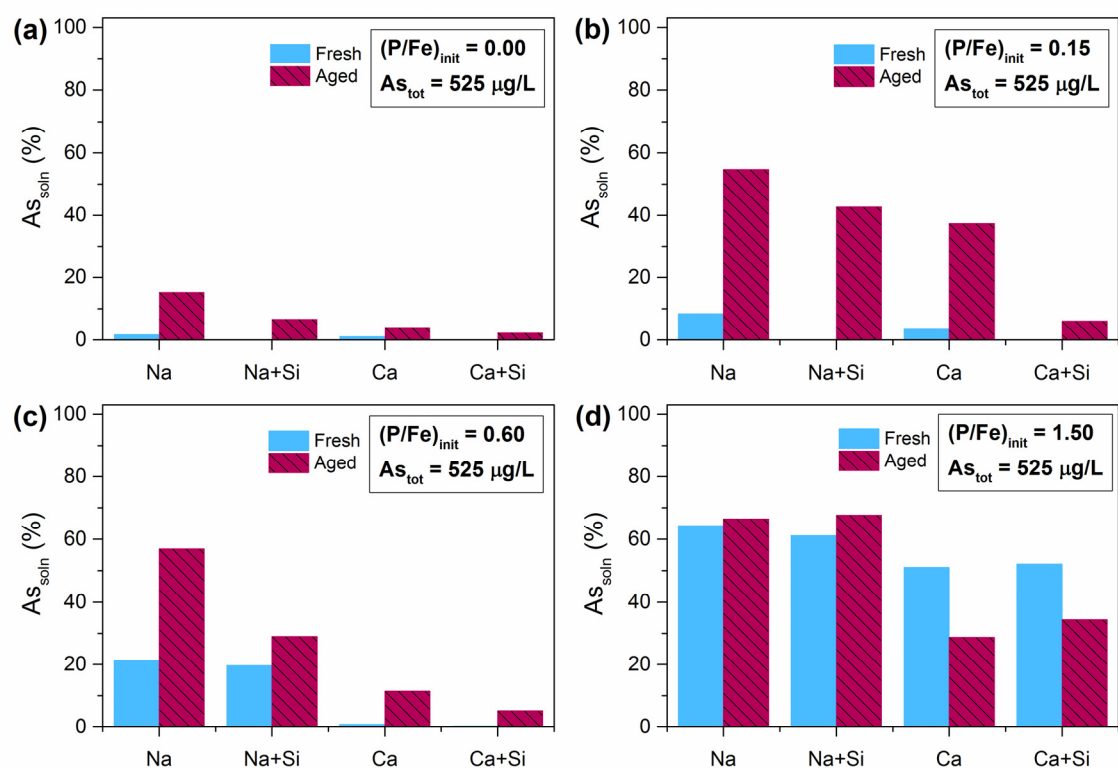


Figure 2. Dissolved As(V) in fresh (a,c) and aged (b,d) suspensions as a function of $(P/Fe)_{init}$; in percent of initially spiked amounts on linear scale (a, b; all electrolytes) and in absolute concentration units ($\mu g/L$) on a logarithmic scale (c, d; Na, Ca, Na+Si and Ca+Si electrolytes). Horizontal lines in (c, d) mark the initial total As(V) concentration (dash-dot), 50 $\mu g/L$ (dot; Bengali drinking water limit) and 10 $\mu g/L$ (dash; WHO drinking water limit). Thin vertical lines in (a, c) indicate the $(P/Fe)_{crit}$ of the individual electrolytes (from Senn et al. (2015)). The arrows in panel (c) indicate the marked effects of Si (green) and Ca (blue) on residual dissolved As concentrations in the fresh suspensions.



730

731 Figure 3. Dissolved total As (As_{soln}) (% of total initial As(V)) in fresh and aged precipitate
 732 suspensions at (nominal) $(P/Fe)_{init}$ of 0.00, 0.15, 0.60 and 1.50 in Na, Na+Si, Ca, and Ca+Si
 733 background electrolyte. Values at $(P/Fe)_{init}$ 0.15 are an average of data from $(P/Fe)_{init}$ 0.10
 734 and 0.20.

735

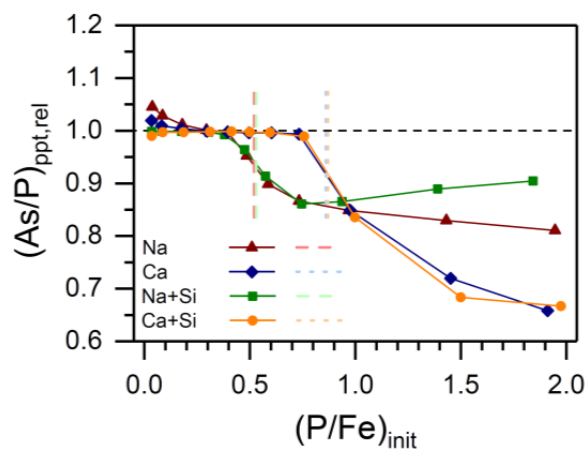


Figure 4. Relative precipitate As/P ratio $(As/P)_{ppt,rel}$ in the Na, Ca, Na+Si and Ca+Si electrolytes as a function of $(P/Fe)_{init}$. The $(As/P)_{ppt,rel}$ corresponds to the ratio between the molar $(As/P)_{ppt}$ and the initial molar As/P ratio in solution $((As/P)_{init})$. Values >1 indicate preferential uptake of As(V) over P, values <1 suggest preferential uptake of P. The thin vertical lines indicate the $(P/Fe)_{crit}$ of the different electrolytes (from Senn et al. (2015)).

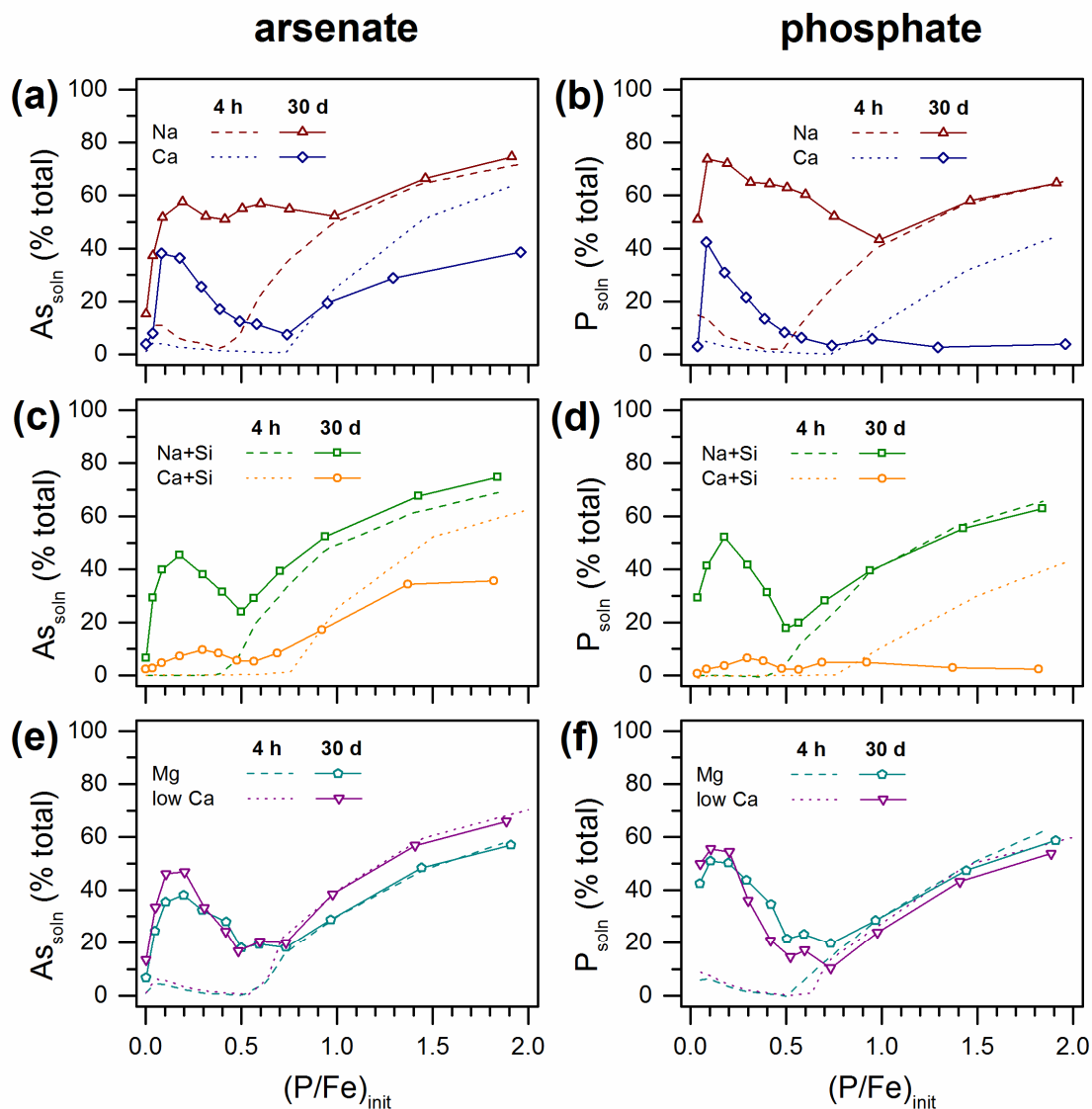


Figure 5. Dissolved As (a,c,e) and P (b,d,f) fractions in aged suspensions in percent of initially spiked amounts as a function of $(P/Fe)_{init}$ in Na, Ca, Na+Si, Ca+Si, low Ca and Mg background electrolytes (symbols and solid lines). The corresponding concentrations in fresh suspensions from Figure 2 are shown for comparison (dotted lines). Data for dissolved P from Senn et al. (2015) and Senn et al. (2017).

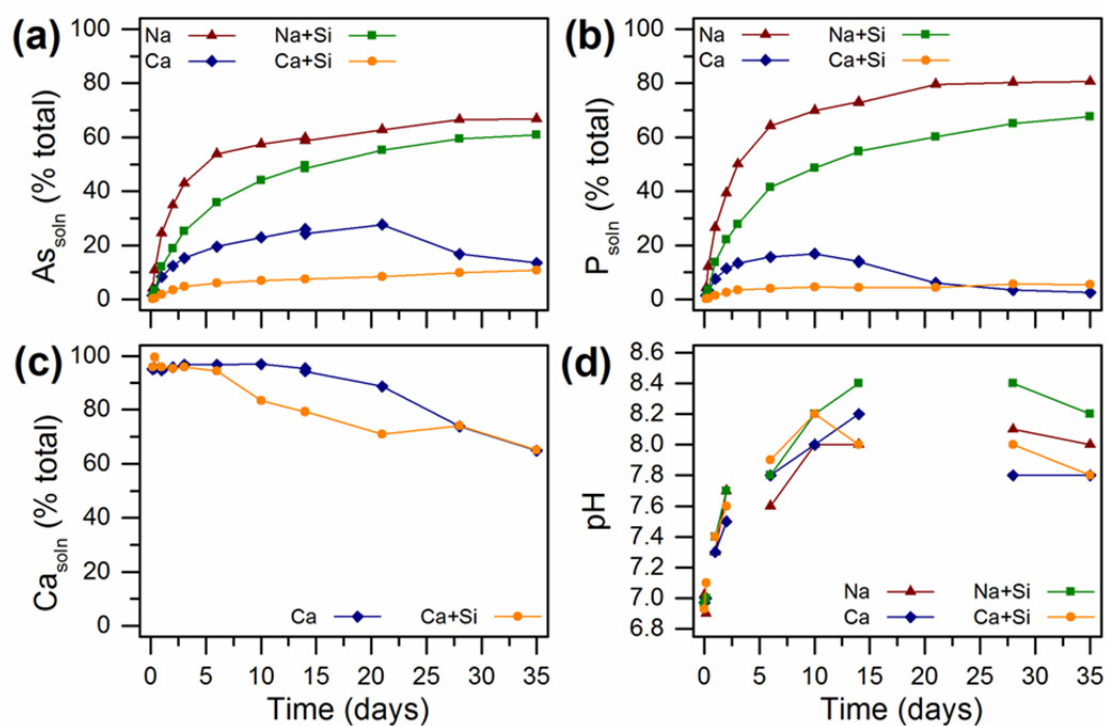
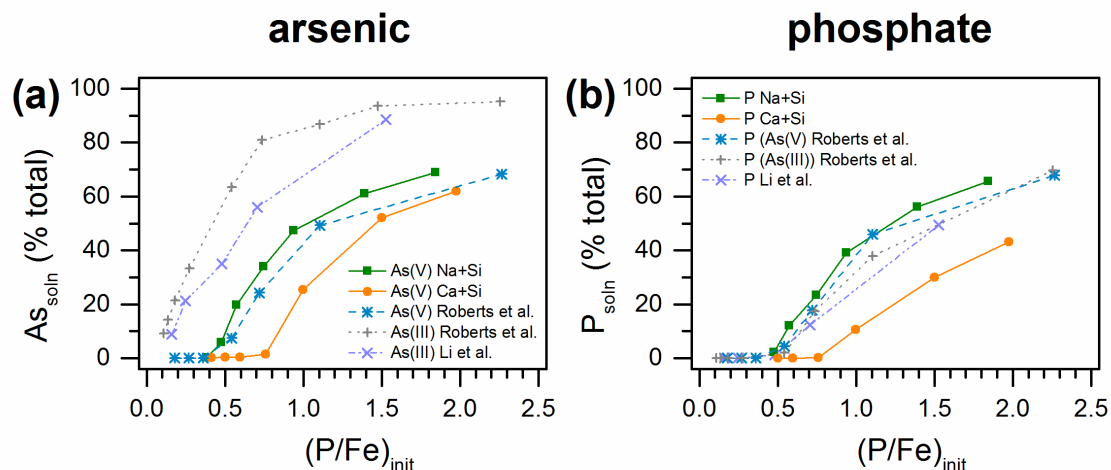


Figure 6. Time-resolved aging experiment at $(P/Fe)_{init}$ of 0.25 (Fe_{tot} 0.56 mM) in Na, Na+Si, Ca, and Ca+Si electrolyte. Fractions of dissolved As(V) (a), dissolved P (b) and dissolved Ca (c) and solution pH (d).



757

758 Figure 7. Data for residual dissolved As and P as a function of $(P/Fe)_{init}$ from co-precipitation
 759 experiments in synthetic Bangladesh groundwater (SBGW) from Roberts et al. (2004) (6.7
 760 μ M As(V) or As(III), 1.07 mM Si, 97 μ M P, 2.5 mM Ca, 1.5 mM Mg, Fe(II) from 50 to 0.04
 761 mM, pH 7.0) and from electrocoagulation experiments with As(III) in SBGW from Li et al.
 762 (2012) (6.7 μ M As(III), 1.07 mM Si, 97 μ M P, 2.5 mM $CaCl_2$, 1.6 mM $MgCl_2$, 8.2 mM
 763 $NaHCO_3$) in comparison to the data for As(V) and P in the fresh Na+Si and Ca+Si
 764 electrolytes (from Figure 2). Note that residual dissolved As corresponds to a mixture of
 765 As(III) and As(V) in experiments with As(III), and to As(V) in experiments with As(V).

Supplementary Data

Arsenate co-precipitation with Fe(II) oxidation products and retention or release during precipitate aging

Anna-Caterina Senn^{a,b}, Stephan J. Hug^a, Ralf Kaegi^a, Janet G. Hering^{a,b,c}, Andreas Voegelin^{a,}*

^a Eawag, Swiss Federal Institute of Aquatic Science and Technology, Ueberlandstrasse 133, CH-8600 Dübendorf, Switzerland

^b Department of Environmental Sciences, Institute of Biogeochemistry and Pollutant Dynamics, ETH, Swiss Federal Institute of Technology, Zurich, Switzerland

^c School of Architecture Civil and Environmental Engineering, EPFL, École Polytechnique Fédérale de Lausanne, Switzerland

* Corresponding author. E-mail address: andreas.voegelin@eawag.ch, phone +41 58 765 54 70, fax +41 58765 52 10

(5 pages, 1 table, 2 figures)

Solution composition in co-precipitation experiments

Table S1. Conditions of co-precipitation experiments used for parameter optimization in our study and in Roberts et al. (2004).

	This study			Roberts et al., 2004
	Na / Na+Si	Ca / Ca+Si	Mg / low Ca	SBGW ^a
pH_{init}	7.0 ± 0.1	7.0 ± 0.1	7.0 ± 0.1	7.0 ± 0.1
HCO₃^{-b}	8	8	8	8
Na^c	8	---	--- / 7	---
Ca (mM)	---	4	--- / 0.5	2.5
Mg (mM)	---	---	4 / ---	1.6
Si (mM)	--- / 0.5	--- / 0.5	---	1.07
P (mM)	0.2 / 0 – 1 ^c	0.2 / 0 – 1 ^c	0.2 – 1 ^c	0.097
As (μM)	7	7	7	6.67
Fe (mM)	0.5	0.5	0.5	0.04 – 0.9
(P/Fe)_{init}^d	0.4 / 0 – 2 ^c	0.4 / 0 – 2 ^c	0.4 – 2 ^c	0.11 – 2.38
(As(V)/Fe)_{init}	0.014	0.014	0.014	0.01 – 0.16
(Si/Fe)_{init}	--- / 1	--- / 1	---	2 – 25
(Ca/Fe)_{init}	---	8	--- / 1	4.7 – 58.6

^aSynthetic Bangladesh groundwater.

^bBased on thermodynamic calculations, adjustment of the pH to 7.0 required equilibration with 38 mbar CO₂ and resulted in 9.5 mM total bicarbonate.

^cNa added as NaHCO₃. Spiking with 0.5 mM Si (as Na₂SiO₃×9H₂O) and up to 1 mM P (as NaH₂PO₄·H₂O), resulted in further Na additions of 1 mM and up to 1 mM, respectively.

^dFor Si-free electrolytes, data from treatments with (P/Fe)_{init} of 0 to 0.3 were omitted in model parameter refinement.

Recovery of total As in fresh and aged suspensions

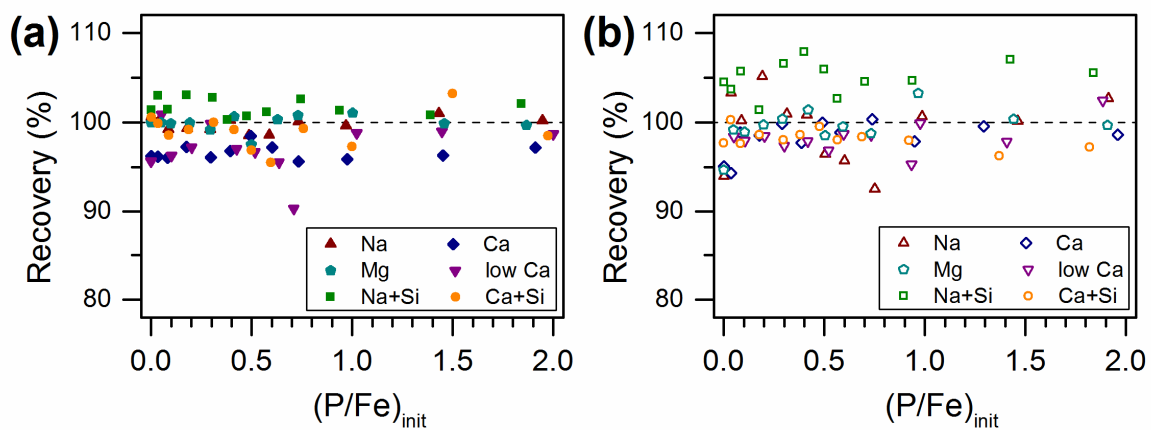


Figure S1. Recoveries of total As in the reaction suspensions after 4 hours (a) and 30 days (b) reaction times for the six different background electrolytes. Recovery was calculated by dividing total As after 4 hours or 30 days by the total initial As.

Correction for colloidal P and As(V) in fresh and aged Na and Na+Si electrolytes

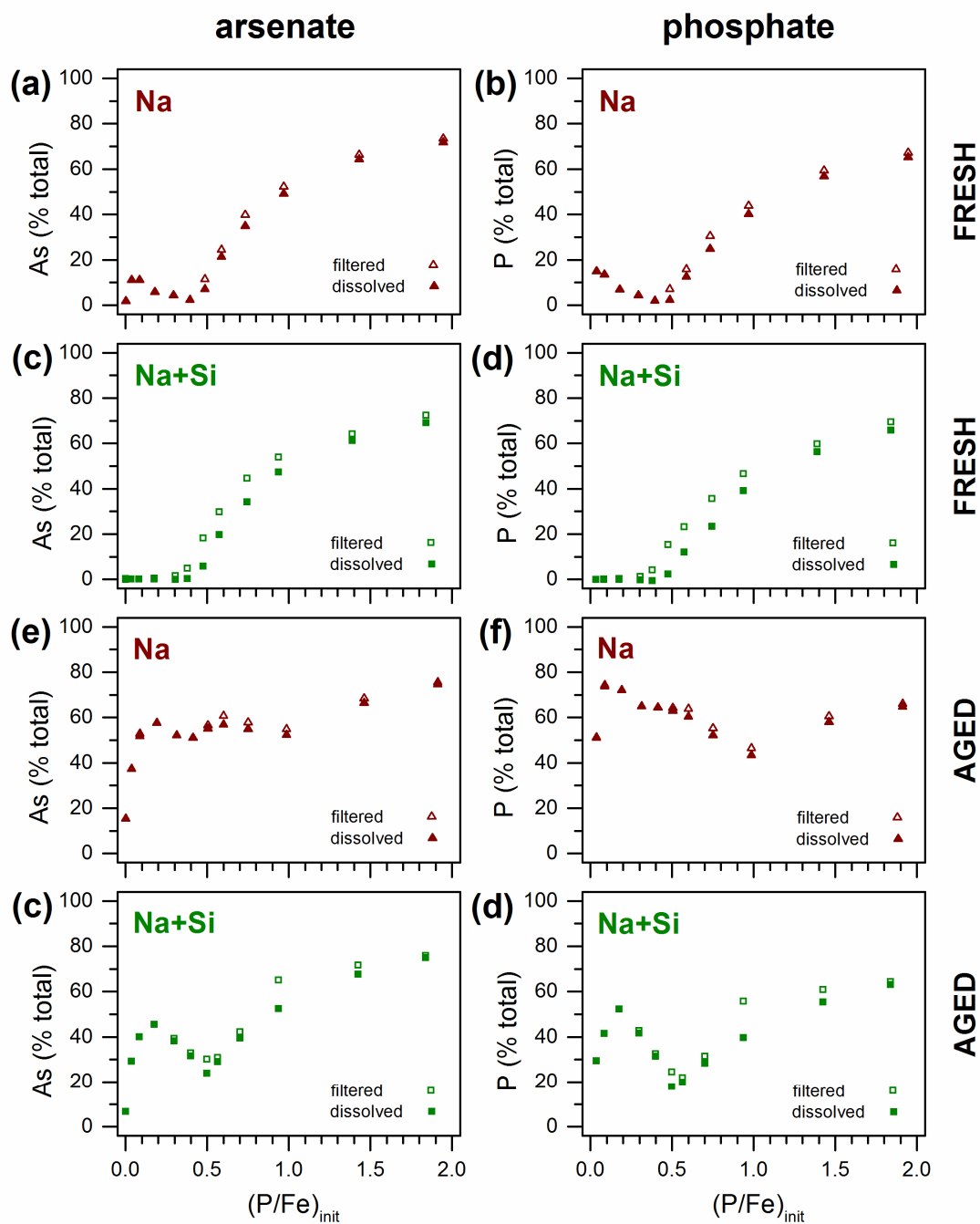


Figure S2. Comparison of measured concentrations of P and As(V) in filtered suspensions from the fresh and aged Na and Na+Si electrolytes and dissolved concentrations obtained by correcting for colloidal P and As(V) (see text for details), expressed as percentage of total P and As(V) in suspension.

For the aged Na and Na+Si electrolytes, colloidal As or P typically accounted for $\leq 10\%$ of the As_{filt} and P_{filt} , respectively, except for the treatments Na+Si 0.5 A and Na+Si 1.0 A, where $X_{\text{coll}}/X_{\text{filt}}$ ranged between 20% and 29%. In the fresh Na and Na+Si electrolytes, the concentrations X_{filt} decreased from $\sim 67\text{-}71\%$ at $(P/Fe)_{\text{init}}$ of ~ 2 to $7\text{-}18\%$ at $(P/Fe)_{\text{init}}$ of ~ 0.5 (in percent of total concentrations). Concomitantly, the estimated fraction of colloidal As and P in the filtered suspensions ($X_{\text{coll}}/X_{\text{filt}}$) increased from 2-5% to 40-85%. In fresh Na electrolyte suspensions with $(P/Fe)_{\text{init}}$ of 0.4 and lower, colloidal As and P were negligible ($X_{\text{coll}}/X_{\text{filt}} \leq 2\%$). For the fresh Na+Si electrolyte, on the other hand, the correction suggested that essentially all As_{filt} and P_{filt} at $(P/Fe)_{\text{init}}$ of 0.4 and 0.3 was in colloidal form. For lower $(P/Fe)_{\text{init}}$ from 0.3 to 0, the concentrations of Fe, P and As in the filtered suspensions were too low for a reliable estimation of the colloidal and dissolved fractions. However, filterable As and P concentrations corresponding to $< 0.3\%$ of their total spiked concentrations indicated the upper limit of dissolved As and P. Based on these considerations, the dissolved concentrations of As and P in fresh Na+Si electrolyte suspensions with $(P/Fe)_{\text{init}} \leq 0.5$ were set to zero for plots and data modeling on a linear scale, and were omitted in plots on a logarithmic scale.